The Chromatin Remodeling Component *Arid1a* Is a Suppressor of Spontaneous Mammary Tumors in Mice

Nithya Kartha, Lishuang Shen,[1] Carolyn Maskin, Marsha Wallace,[2] and John C. Schimenti[3]
Department of Biomedical Sciences, College of Veterinary Medicine, Cornell University, Ithaca, New York 14853

ABSTRACT Human cancer genome studies have identified the SWI/SNF chromatin remodeling complex member *ARID1A* as one of the most frequently altered genes in several tumor types. Its role as an ovarian tumor suppressor has been supported in compound knockout mice. Here, we provide genetic and functional evidence that *Arid1a* is a *bona fide* mammary tumor suppressor, using the Chromosome aberrations occurring spontaneously 3 (*Chaos3*) mouse model of sporadic breast cancer. About 70% of mammary tumors that formed in these mice contained a spontaneous deletion removing all or part of one *Arid1a* allele. Restoration of *Arid1a* expression in a *Chaos3* mammary tumor line with low *Arid1a* levels greatly impaired its ability to form tumors following injection into cleared mammary glands, indicating that ARID1A insufficiency is crucial for maintenance of these *Trp53*-proficient tumors. Transcriptome analysis of tumor cells before and after reintroduction of *Arid1a* expression revealed alterations in growth signaling and cell-cycle checkpoint pathways, in particular the activation of the TRP53 pathway. Consistent with the latter, *Arid1a* reexpression in tumor cells led to increased *p21* (*Cdkn1a*) expression and dramatic accumulation of cells in G2 phase of the cell cycle. These results not only provide *in vivo* evidence for a tumor suppressive and/or maintenance role in breast cancer, but also indicate a potential opportunity for therapeutic intervention in ARID1A-deficient human breast cancer subtypes that retain one intact copy of the gene and also maintain wild-type TRP53 activity.

KEYWORDS *Arid1a*; tumor suppressor; breast cancer; cell cycle; senescence; mouse

THE identification of genetic drivers of specific types and subtypes of cancer continues to be an important goal of cancer biology research. Major efforts including The Cancer Genome Atlas (TCGA) project have cataloged mutations in diverse human tumors. This wealth of data has been instrumental in identifying genes that may be playing a direct or indirect role in carcinogenesis by virtue of their being commonly altered in a particular cancer type. However, proving causality of these candidate "driver" genes, and elucidating their roles in tumorigenesis, requires relevant experimental validation.

doi: 10.1534/genetics.115.184879
Manuscript received January 18, 2016; accepted for publication June 4, 2016; published Early Online June 8, 2016.
Supplemental material is available online at www.genetics.org/lookup/suppl/doi:10.1534/genetics.115.184879/-/DC1.
[1]Present address: Center for Personalized Medicine, Children's Hospital of Los Angeles, Los Angeles, CA, 90057.
[2]Present address: Nuffield Department of Medicine, Ludwig Institute for Cancer Research, University of Oxford, Oxford, UK, OX3 7DQ.
[3]Corresponding author: Department of Biomedical Sciences, College of Veterinary Medicine, Cornell University, Ithaca, NY 14853. E-mail: jcs92@cornell.edu

ARID1A (also called *BAF250a*), encoding an important component of the mammalian SWI/SNF complex, has emerged as one of the most commonly mutated or downregulated genes in diverse tumors, including gastrointestinal (Wang *et al.* 2011; Cajuso *et al.* 2014), endometrial (Liang *et al.* 2012; The Cancer Genome Atlas Research Network *et al.* 2013), ovarian clear cell (Jones *et al.* 2010; Wiegand *et al.* 2010), pancreatic (Waddell *et al.* 2015), lung (Imielinski *et al.* 2012), and breast (Cornen *et al.* 2012; Mamo *et al.* 2012). ARID1A impacts epigenetic gene regulation by altering chromatin structure around promoters of specific loci in conjunction with its associated SWI/SNF complex components (Inoue *et al.* 2011; Chandler *et al.* 2013). Therefore, its downregulation or mutation in somatic cells can have profound consequences, including inappropriate proliferation (Romero and Sanchez-Cespedes 2014). Despite the accumulating correlative data implicating *ARID1A* as a tumor suppressor, functional proof has been lacking in part due to the fact that knockout of *Arid1a* in mice causes embryonic lethality even in the heterozygous state (Gao *et al.* 2008). However, two recent reports have shown that conditional

biallelic knockout of *Arid1a* in ovarian surface epithelial cells, in conjunction with either conditional expression of a mutant phosphoinositide 3-kinase catalytic subunit (PIK3CA) (Chandler *et al.* 2015), or conditional disruption of *Pten* (Guan *et al.* 2014), caused carcinomas resembling clear cell in the former, and endometriod/undifferentiated in the latter. In both studies, deletion of *Arid1a* alone, or deletion of only one *Arid1a* allele in the compound mutant situations, was insufficient to cause cancer. While these studies provided compelling evidence for the tumor suppressive role of *Arid1a* in ovarian cancer, they (and most other genetically engineered cancer models) do not model the process of sporadic cancer development. Furthermore, the dependency of biallelic *Arid1a* inactivation upon mutation of *Pten* or *Pik3ca* in driving tumor formation in these models seems to be specific to the pathogenesis of endometrium-related ovarian neoplasms (Maeda and Shih Ie 2013) and does not appear to apply to several of the other human cancers in which *ARID1A* is commonly mutated (Kandoth *et al.* 2013). Thus, it is important to validate cancer genes/pathways in the context of their tumor-type-specific environments, as the behavior of these genes and pathways may vary by tissue type. Sporadic breast cancer (*i.e.*, not associated with inherited neoplasia-driving mutations) accounts for the vast majority of breast cancer cases in the U.S. (80–85%) (American Cancer Society 2014). Although *ARID1A* has not yet been widely recognized as a key suppressor of breast carcinogenesis, it is heterozygously deleted in a substantial fraction of tumors (Cornen *et al.* 2012; Mamo *et al.* 2012), and low *ARID1A* expression in tumors of patients with breast cancer correlates significantly with poorer prognosis and overall survival (Mamo *et al.* 2011; Zhao *et al.* 2014; Cho *et al.* 2015; Zhang *et al.* 2015). Here, we report functional evidence that *Arid1a* loss is critical for mammary tumorigenesis in a mouse model of spontaneous breast cancer and present data on how this leads to deregulated cancer cell growth.

Results and Discussion

The *Chaos3* mouse, bearing a missense allele ($Mcm4^{Chaos3}$) of the DNA replication gene *Mcm4*, exhibits high levels of genomic instability caused by the mutation's destabilization of the MCM2–7 replicative helicase complex (Shima *et al.* 2007; Kawabata *et al.* 2011; Chuang *et al.* 2012). Most females homozygous for the *Chaos3* mutation congenic in the C3HeB/FeJ strain background (C3H-*Chaos3*) develop spontaneous mammary tumors (MTs) with an average latency of 12 months (Shima *et al.* 2007). Array Comparative Genomic Hybridization (aCGH) analyses of nine C3H-*Chaos3* MTs revealed interstitial deletions common to a small number of chromosomal regions (Wallace *et al.* 2012). Almost all tumors were missing both copies of *Nf1*, a tumor suppressor that functions as negative regulator of *Ras*, but positive for *Trp53* (Wallace *et al.* 2014).

Those aCGH data, plus an additional 12 reported here, indicated that most (18/21) MTs also contained deletions involving part or all of an ~100-kb region on chromosome 4 (Chr4) (Figure 1) containing *Arid1a* (Figure 1). To further validate the aCGH results, we performed digital droplet PCR (ddPCR) on DNA from the same 12 MTs plus three non-MTs using probes situated at both ends of *Arid1a*. All 15 calls for probe 2, and 13/15 for probe 1 (Figure 1A) were consonant. The two discrepancies were in MTs 7 and 12, which according to aCGH results, have an identical deletion breakpoint within *Arid1a*. It is possible that in these cases, the breakpoint is actually proximal to that called by the software. As an alternative confirmation of *Arid1a* hemizygosity in these tumors, we took advantage of genetic polymorphisms in two F_1 (C3HeB/FeJ × C57BL/6J) MTs deleted for *Arid1a* (Figure 1, nos. 1 and 8) and an F_2 MT having no deletion (Figure 1, no. 2), based on aCGH calls. Genotyping of SNPs at the 3′ end of *Arid1a* revealed agreement with the aCGH and ddPCR data (Figure 1A and Supplemental Material, Figure S1).

We next scored 33 additional C3H-*Chaos3* MTs and five cell lines derived from C3H-*Chaos3* MTs for deletions in the *Arid1a* coding region by ddPCR. In total, ~70% of the *Chaos3* MTs analyzed had monoallelic deletions for all or part of *Arid1a* (Table S1). Hemizygosity for *ARID1A* also appears to be common in human breast carcinomas at frequencies as high as ~40% depending on the dataset (The Cancer Genome Atlas Network 2012; Ciriello *et al.* 2015; Eirew *et al.* 2015) (Figure S2).

If hemizygosity of *Arid1a* contributes to tumorigenesis, then either it is haploinsufficient (*i.e.*, 50% expression contributes to the transformed state) or the nondeleted allele is also altered in a genetic or epigenetic manner that reduces *Arid1a* expression to a level below that which is necessary to prevent transformation and/or tumor growth. To test this, we quantified *Arid1a* messenger RNA (mRNA) in hemizygous and nondeleted C3H-*Chaos3* MTs. On average, transcript levels in 24 *Arid1a*-deleted tumors, but not nondeleted tumors, was about half that present in WT mammary tissue (Figure 2 and Table S2). The results suggest that ARID1A reduction, but not elimination, may contribute to tumorigenesis or tumor maintenance. Interestingly, the two *Chaos3* non-MTs tested had approximately fivefold more *Arid1a* than the deleted MTs (Figure 2).

The genetic and molecular data described above imply, but do not prove, that decreased ARID1A expression is involved in either neoplastic transformation or maintenance of the transformed state. To address this question functionally, we conducted experiments to restore *Arid1a* expression in ARID1A-deficient C3H-*Chaos3* MT cells, followed by analyses of the *in vitro* and *in vivo* consequences. First, we generated a *Chaos3* MT cell line (23116 MT) that has one copy of *Arid1a* deleted (Table S1) and very low levels of *Arid1a* expression (Figure 3, A and B), and then stably introduced an *Arid1a* complementary DNA (cDNA) expression construct into these cells using lentivirus-mediated transduction. These transformed lines were termed "Addback" (AB) cells. We then

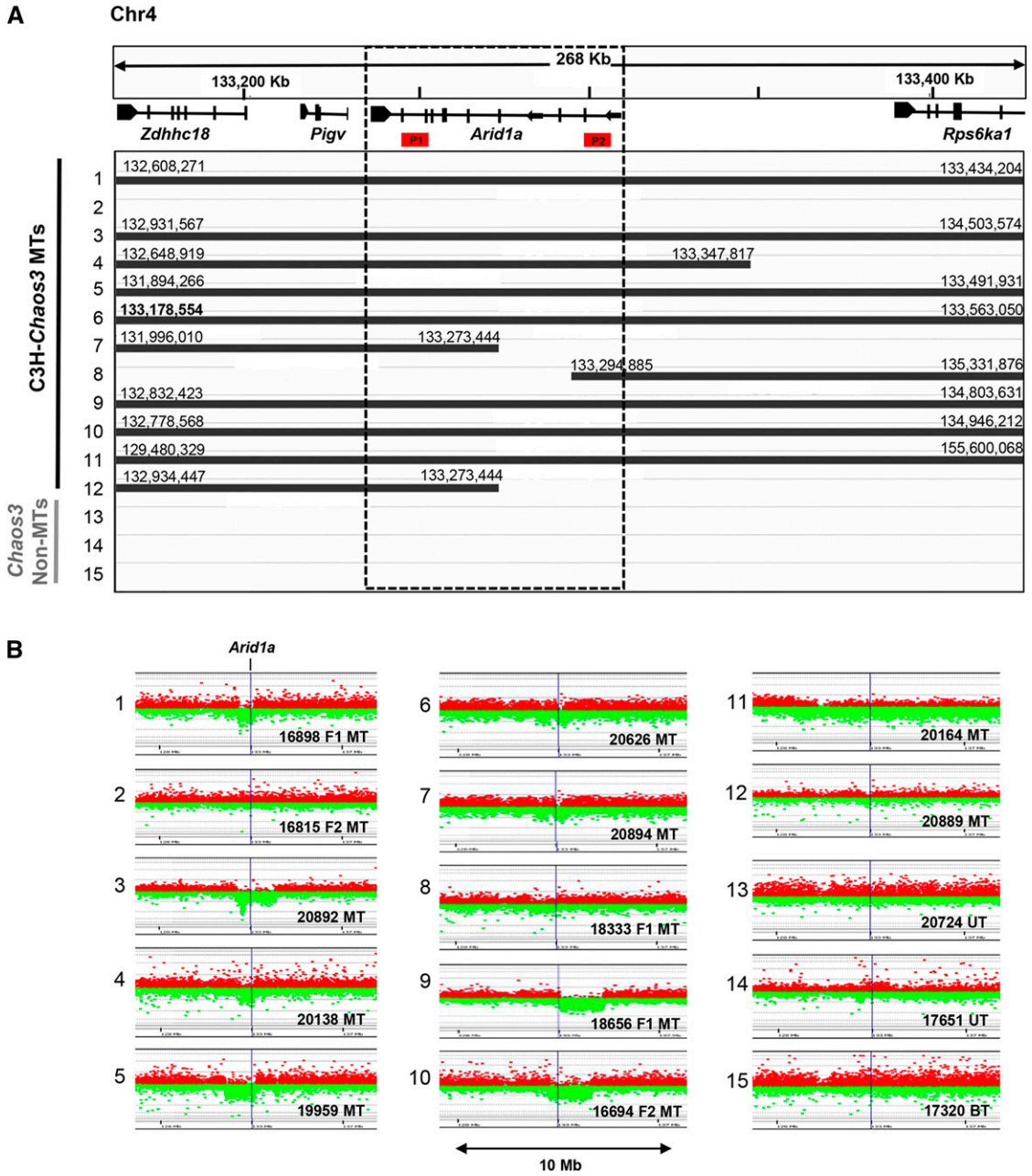

Figure 1 *Arid1a* is recurrently deleted in C3H-*Chaos3* mammary tumors. (A) Overview of aCGH data near the *Arid1a* locus from 15 tumor samples, adapted from an IGV depiction. Solid lines denote stretches of contiguous probes with reduced hybridization signal, thus representing deleted regions. Nucleotide coordinates of deletion endpoints are indicated and correspond to the last probe with reduced hybridization signal on the array. The control non-MTs consist of two uterine tumors and one bone tumor. (B) Plot of probe intensities near the *Arid1a* from aCGH hybridization. Each dot is a probe on the array, with the green and red representing control *vs.* tumors, respectively. Locations of primer pairs used for *Arid1a* CNV analyses by ddPCR are depicted as P1 and P2 (see *Materials and Methods*). MT, mammary tumor.

assessed cell proliferation activity via 5-ethynyl-2′-deoxyuridine (EdU) incorporation in the parental *vs*. three transduced cell lines, and found that ectopic *Arid1a* expression caused a dramatic decrease (approximately threefold) in EdU incorporation in each of the lines tested (Figure 3C).

To determine if ARID1A is required for tumorigenicity, we tested whether one of the transduced clones (AB-C1) exhibiting elevated levels of mRNA (Figure 3A) and protein (Figure 3B) would reduce/abolish the ability of 23116 MT cells to form tumors when transplanted into host animals. The parental and AB-C1 cancer cells were injected into cleared mammary fat pads of WT C3H female mice (23116 MT on one side and AB-C1 on the other of each mouse; see *Materials and Methods*) and monitored for tumor formation. Overexpression of *Arid1a* significantly decreased MT formation frequency and size (Figure 3D). These results indicate that loss/reduction of *Arid1a* expression is crucial for the growth and/or formation of C3H-*Chaos3* MTs. As shown

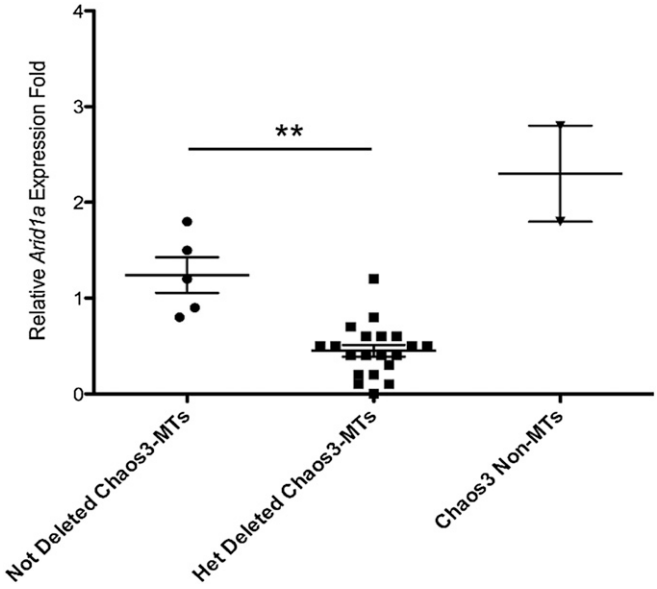

Figure 2 Tumors hemizygous for *Arid1a* have less *Arid1a* mRNA. Plotted are qRT-PCR expression data from the *Chaos3* non-MTs (two uterine tumors) and C3H-*Chaos3* MTs that were either heterozygously deleted (n = 21) or not deleted (n = 5) for *ARID1A*, based on ddPCR data. Expression levels for each sample were calculated relative to an average of two WT RNA tissue samples. Significant differences were calculated using a two-tailed Student's t-test (** $P < 0.001$).

below, ectopic *Arid1a* overexpression did not inhibit tumor formation in an unrelated non-*Chaos3* MT cell line MCN1, indicating that excessive ARID1A itself is not cell toxic.

To gain insight into the mechanisms by which *Arid1a* loss promotes tumorigenesis in the *Chaos3* model, we considered data showing that *Arid1a* is required for efficient functioning of the DNA damage response (DDR), specifically the G2/M cell-cycle checkpoint that helps suppress genomic instability (GIN) and tumorigenesis (Lobrich and Jeggo 2007; Shen *et al.* 2015). Since *Chaos3* cells have chronic replication stress and GIN (Shima *et al.* 2007; Kawabata *et al.* 2011; Bai *et al.* 2016), it is possible that a loss or reduction of ARID1A in a cell allows escape from DDR-mediated growth arrest or apoptosis, thus promoting carcinogenesis. Therefore, we examined the cell cycle of AB-C1 cultures. This revealed an accumulation of cells in the G2 phase (Figure 4, A and B), suggesting that *Arid1a* overexpression might be inducing a checkpoint response and consequent growth arrest.

Since ectopic *Arid1a* expression in ARID1A-deficient MT cells caused cell-cycle arrest, we assessed whether either senescence or apoptosis was triggered as a consequence. TUNEL assays did not reveal a significant increase in apoptosis, based on relative percentages of positively stained cells (23116 MT = 0.6%, ± 0.2% SEM; AB-C1 = 1.5%, ± 0.4%), raising the possibility that these cells were instead senescing. Another indication was the dramatic change in morphological features of the cells in which *Arid1a* was overexpressed. They appeared larger and flatter (Figure 5A), characteristic of cells undergoing senescence (Kuilman *et al.* 2010). Finally, we conducted senescence-associated β-galactosidase (SABG) assays, showing that the AB-C1 cell population had nearly 10-fold more $SABG^+$ cells than the parental cultures (Figure 5, B and C).

Multiple studies have demonstrated that DNA damage-induced G2 arrest activates cellular senescence in a TRP53- and p21-dependent manner (Bunz *et al.* 1998; Mao *et al.* 2012; Krenning *et al.* 2014). mRNA levels of *p21*, which is transcriptionally regulated by TRP53, was approximately fivefold higher in AB-C1 MT cells compared to the 23116 parental line (Figure 5D). Taken together, these data indicate that restoring or overexpressing *Arid1a* in C3H-*Chaos3* MT cells enables G2/M arrest and subsequent cellular senescence. This is consistent with data indicating that ARID1A functions as both a "gatekeeper" in its control of cell proliferation and a "caretaker" in its maintenance of genomic integrity (Wu *et al.* 2014).

To better understand the mechanism by which restoration/overexpression of *Arid1a* impairs growth and tumorigenesis, we conducted RNA sequencing (RNA-seq) comparing the transcriptomes of 23116 MT *vs.* AB-C1 and AB-C2 cells. A total of 554 genes were significantly differentially expressed (DE) between the parental stock and the *Arid1a*-transduced lines [fragments per kilobase of exon per million fragments mapped (FPKM) > 5; $\log_2 > 1$ or < -1 Table S3]. Ingenuity pathway analysis (IPA) of these DE genes revealed that the TRP53 pathway was activated in AB-C1/C2 cells, while the TGFβ pathway was repressed (Figure S3).

RNA-seq data also showed that the most highly upregulated genes within the TRP53 pathway in AB-C1 cells were *Igfbp5*, *Igfbp2*, and *Serpinb2* (*Pai-2*). We validated these data by quantitative RT-PCR (qRT-PCR) (Figure 5E). All three genes have been implicated in tumor growth suppression (Andreasen *et al.* 1997; Butt *et al.* 2003; Pereira *et al.* 2004). *IGFBP5* was found to activate cellular senescence through a TRP53-dependent mechanism in human endothelial cells (Kim *et al.* 2007). These data further support the idea of a TRP53-dependent senescence checkpoint response being activated when *Arid1a* is overexpressed in these cancer cells.

TRP53 was reported to interact physically with ARID1A and the rest of the SWI/SNF complex, enabling transcriptional regulation of downstream gene targets (Guan *et al.* 2011). Several human cancer studies have found that loss of *ARID1A* expression correlates with high amounts of potentially functionally inactive TRP53 (Wang *et al.* 2011; Zang *et al.* 2012; Bosse *et al.* 2013; Bitler *et al.* 2015), suggesting they have codependent tumor suppressive functions, and that ARID1A deficiency would have a similar effect as losing TRP53 activity. A similar mutually exclusive pattern of *Trp53* and *Arid1a* expression seems to exist in C3H-*Chaos3* MTs. They exhibit high levels of TRP53 (Wallace *et al.* 2014), but it does not seem to be effective or functional in the sense of its established role in suppressing uncontrolled cell growth or malignant transformation. Based on this hypothesis as well as the RNA-seq data, it is possible that reexpressing *Arid1a* in the C3H-*Chaos3* tumor cells restores the ability of TRP53 to regulate downstream target genes.

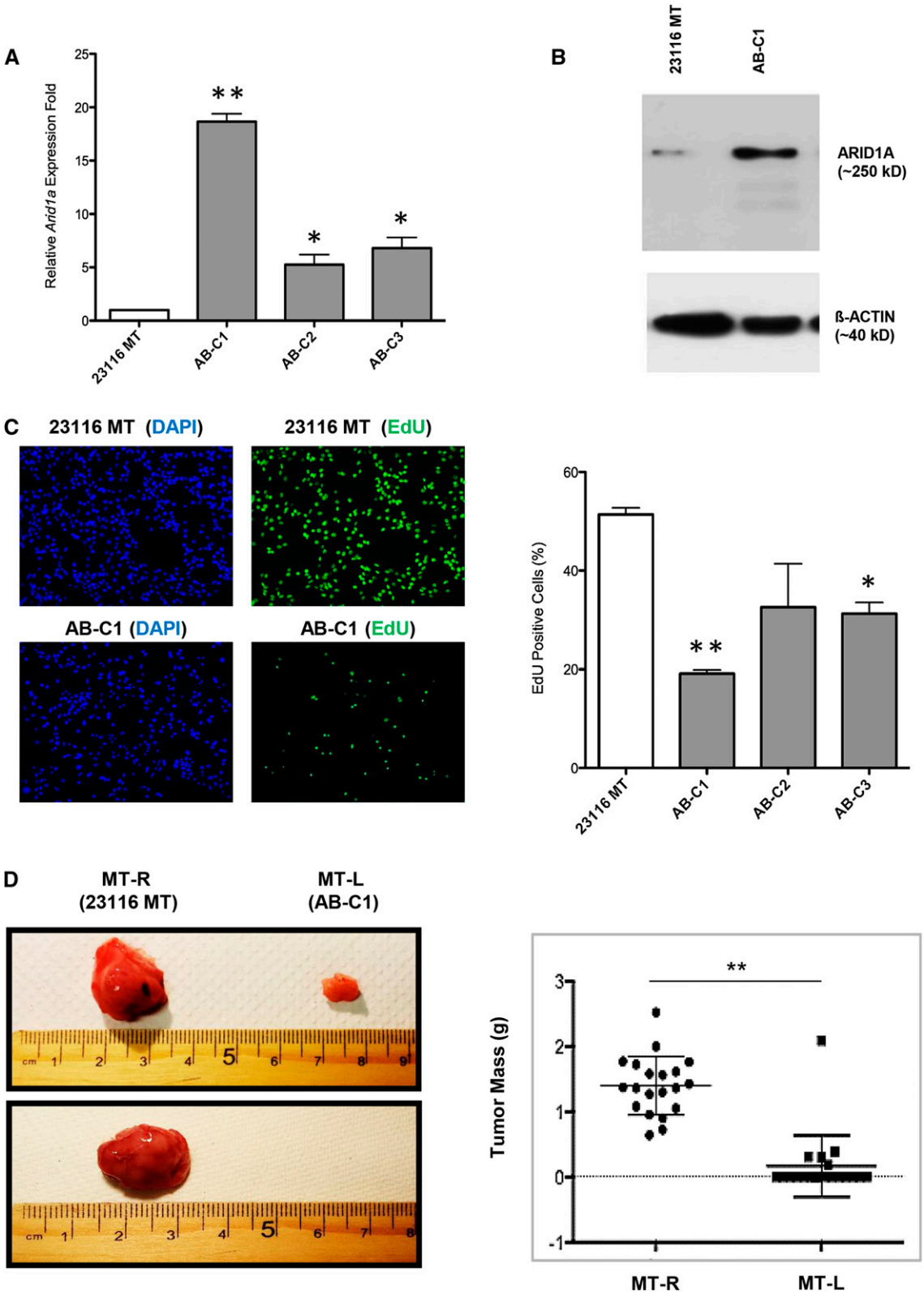

Figure 3 Overexpression of *Arid1a* in C3H-*Chaos3* MT cell line reduces proliferation rate and prevents tumor growth. (A) *Arid1a* expression levels quantified by qRT-PCR in untransduced *Chaos3* MT cell line (23116 MT) and three individual clonal lines (AB-C1, A-C2, and AB-C3) transduced with the *Arid1a* expression vector. Results are shown as the mean ± SEM of three technical replicates. Significant differences were calculated using a two-tailed Student's *t*-test (* $P < 0.05$; ** $P < 0.001$). Values are relative to untransduced parental cell line 23116 MT. (B) *Arid1a* expression levels quantified by immunoblotting in indicated cell lines. (C) EdU incorporation assays of 23116 MT *vs.* AB clones (C1–C3). Error bars signify the mean ± SEM of three experimental replicates, with >1000 cells counted per sample for each replicate. Significant differences were calculated using a two-tailed Student's *t*-test

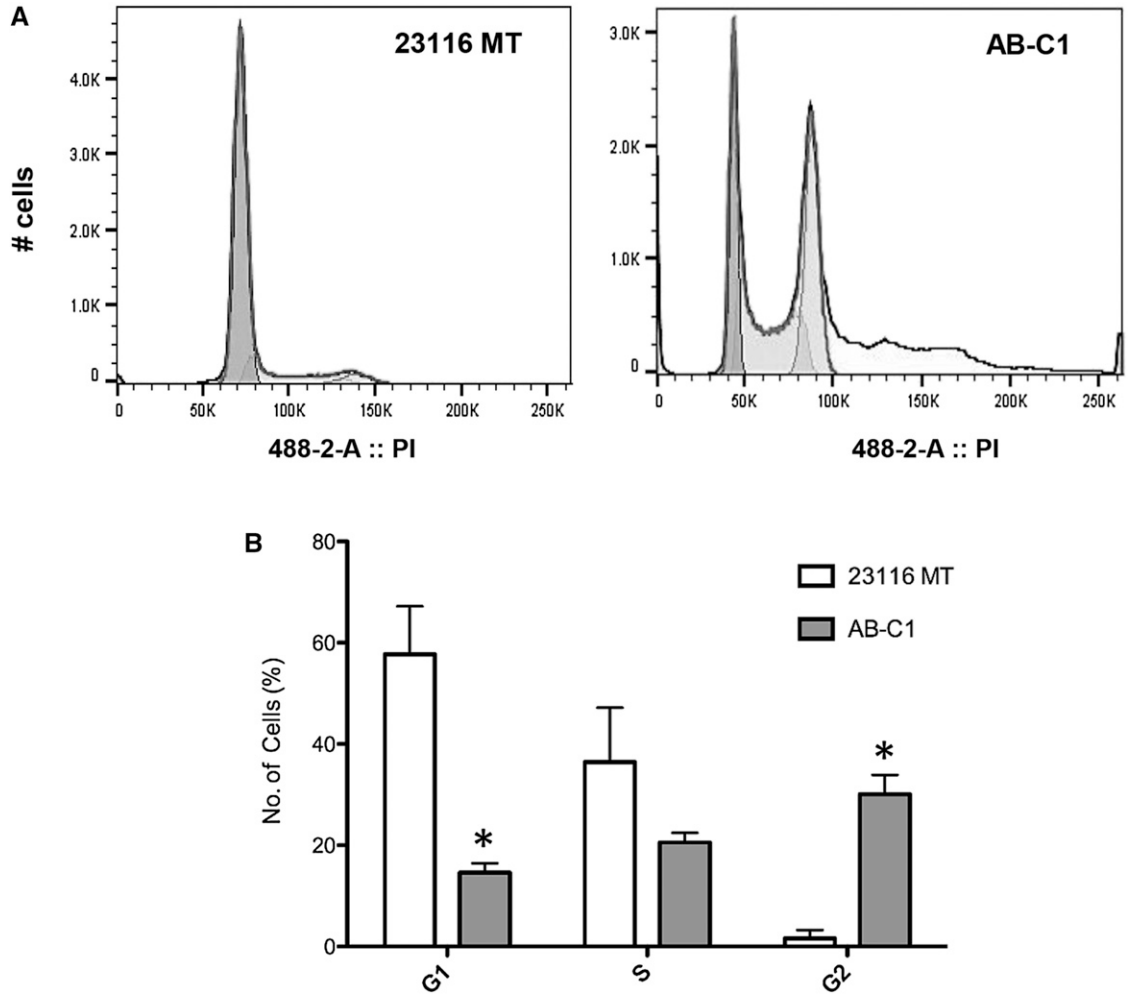

Figure 4 Cell-cycle analysis of C3H-*Chaos3* mammary tumor cell lines. (A) Cell-cycle profiles of 23116 and AB-C1 mammary tumor lines. (B) Percentage of cells in different phases of the cell cycle (G1, S, and G2) based on FloJo statistical analyses. Significant differences were calculated using a two-tailed Student's *t*-test (* $P < 0.05$; ** $P < 0.001$). Values are relative to untransduced parental cell line 23116 MT.

To test this hypothesis, we overexpressed *Arid1a* in a *Trp53* null mouse MT cell line MCN1 (Cheng *et al.* 2010), which we found to not only have low *Arid1a* expression (Figure 6, A and B), but also apparent hemizygosity of *Arid1a* (Table S1). EdU incorporation assays comparing the untransduced and AB cells showed that unlike the TRP53-proficient *Chaos3* cell line 23116, proliferation was unaltered upon overexpressing *Arid1a* in MCN1 (Figure 6C), and subsequent mammary fat pad growth assays revealed that tumorigenecity *in vivo* was also unaffected (Figure 6D). This is consistent with the hypothesis that active TRP53 is necessary for ARID1A to function in its tumor suppressive role.

C3H-*Chaos3* tumors have a manageable number of recurring spontaneous alterations, making it feasible to unravel the molecular events leading to tumor formation—a crucial question in cancer genetics. The experiments here provide genetic and functional evidence that ARID1A is a suppressor of mammary tumorigenesis, and particularly, that it is required for maintenance of tumorigenic potential as revealed by transplantation assays. This role in tumor maintenance also appears to be the case in human ovarian cancer, where it was shown that reintroduction of the gene into tumor cells bearing *ARID1A* mutations inhibited xenograft growth (Guan *et al.* 2011). Our finding that *Arid1a* is almost exclusively monoallelically (not biallelically) deleted in the *Chaos3* model of spontaneous breast cancer, apparently similar to the situation in human breast cancers, is important in terms of potential therapeutic intervention. We showed that overexpressing *Arid1a* ectopically in MT cells greatly suppresses tumor growth in a TRP53-dependent

(* $P < 0.05$; ** $P < 0.001$). Values are relative to untransduced parental cell line 23116 MT. (D) Representative images of tumors (or lack thereof) arising from transplantation of 23116 MT (MT-R) and AB-C1 (MT-L) cells into cleared fad pads of recipient syngeneic C3H females. MT-R and MT-L refer to right and left sides of mouse, respectively (see *Materials and Methods*). Next to it is a plot depicting individual weights of tumors (n = 20 mice, 40 potential tumors). Significant differences between the control and experimental groups were calculated using a two-tailed Student's *t*-test (** $P < 0.001$).

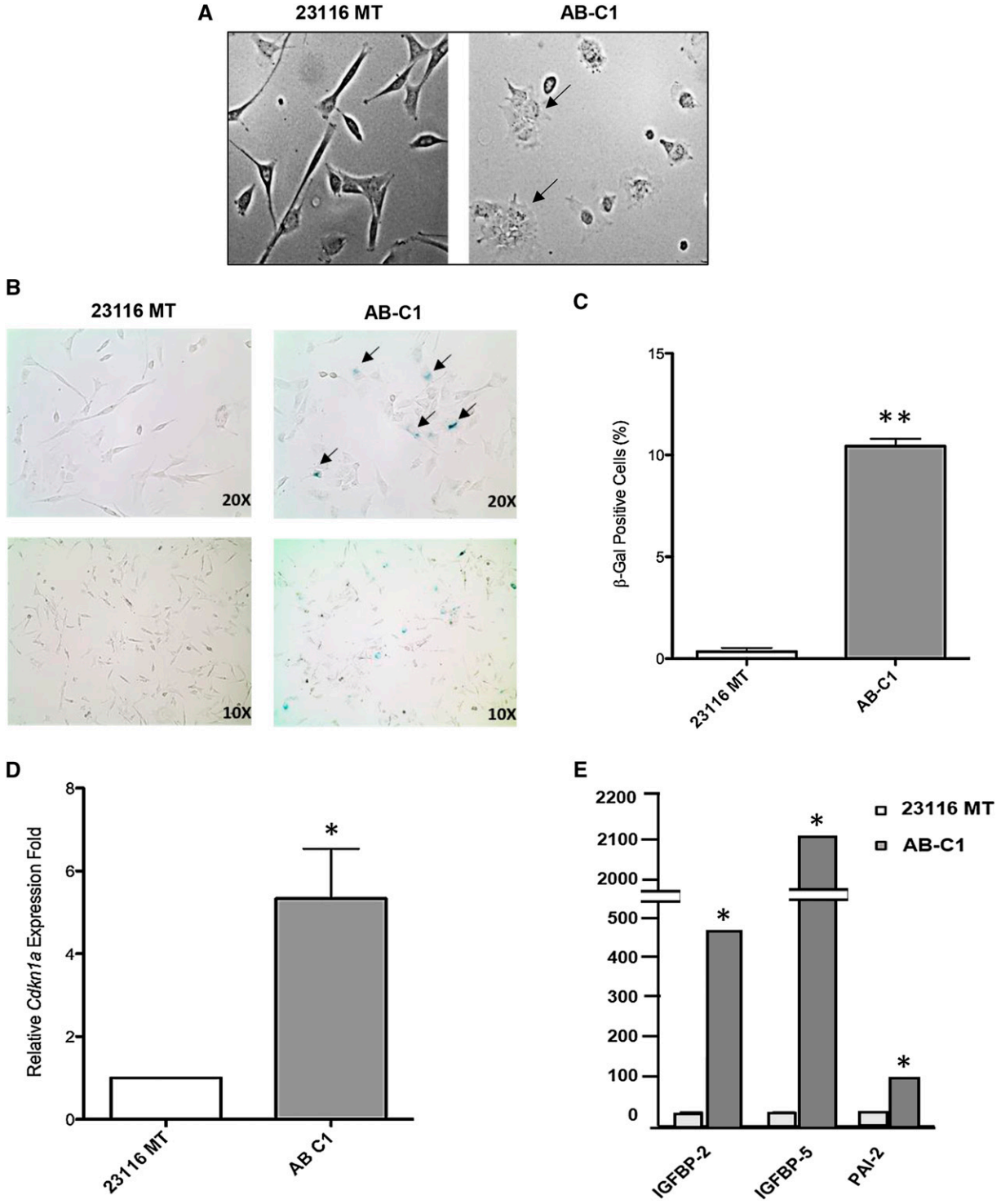

Figure 5 Senescence characteristics of AB-C1 cancer cells. (A) Morphological comparison of 23116 MT *vs.* AB-C1 cells (×20 magnification). (B) Representative images of indicated cells stained for senescence-associated β-galactosidase activity. (C) Average percentages of positively stained cells (blue color) calculated from four technical replicates. (D) qRT-PCR validation of senescence-associated genes. (E) qRT-PCR assay comparing relative transcript levels of *p21* in AB-C1 *vs.* 23116 MT cells. Significant differences were calculated using a two-tailed Student's *t*-test (* $P < 0.05$; ** $P < 0.001$). Values are relative to untransduced parental cell line 23116 MT.

manner. Therefore, in breast cancer cases that retain an intact *ARID1A* allele in *trans* to a mutant/deleted allele, and also contain wild-type (WT) *TRP53*, it may be possible to employ methods for specific reactivation of the remaining allele, thus suppressing tumor growth and triggering cell-cycle arrest. Recent development of sequence-specific, chimeric transcriptional regulators offers one such potential avenue to accomplish this (Maeder *et al.* 2013;

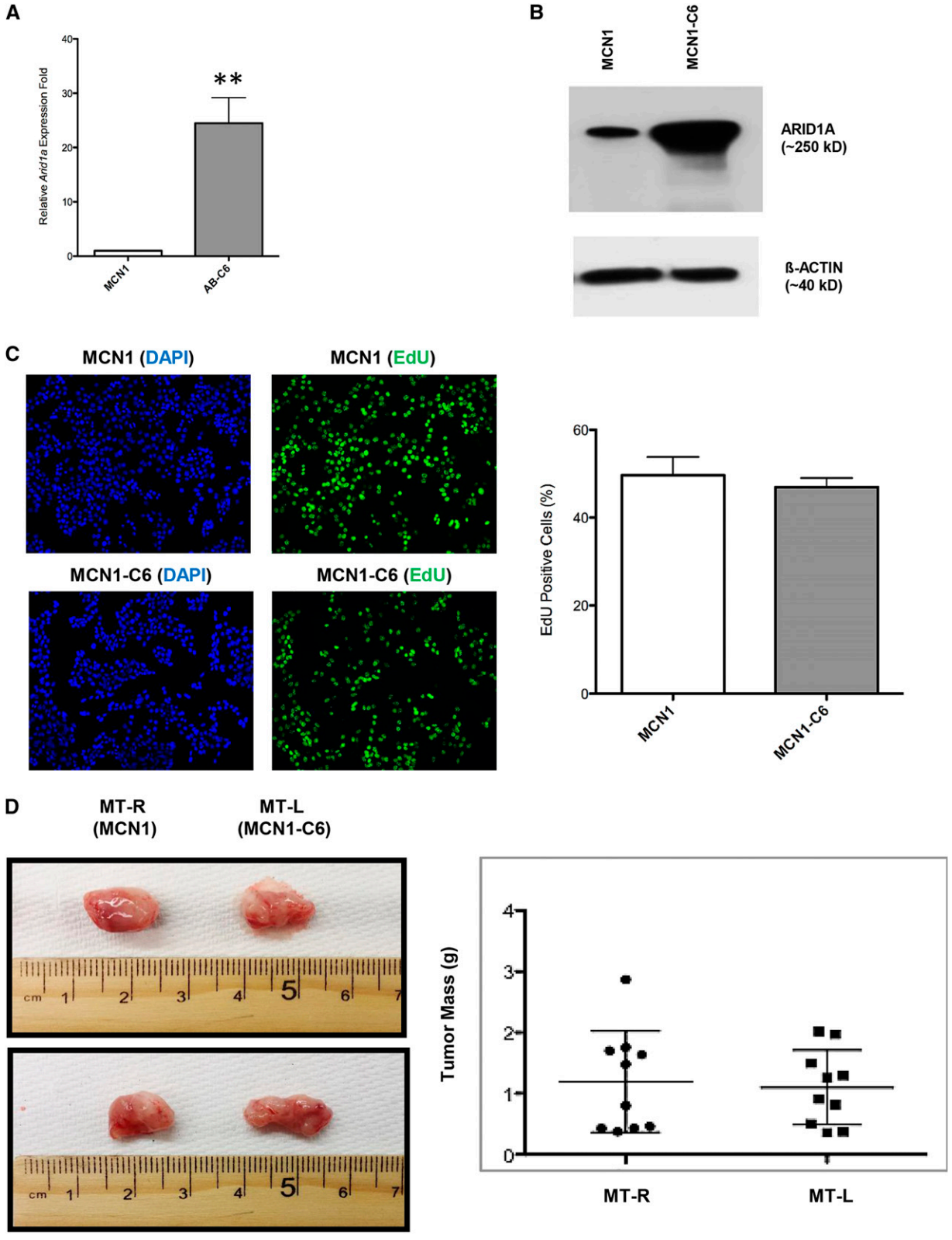

Figure 6 Overexpression of *Arid1a* in the TRP53-deficient MCN1 has no effect on proliferation rate or tumor growth. *Arid1a* expression levels were quantified by (A) qRT-PCR and (B) immunoblotting in MCN1 MT cell line and its transduced counterpart cell line (MCN1-C6). Significant differences were calculated using a two-tailed Student's *t*-test (** $P < 0.001$). Values are relative to untransduced parental cell line MCN1. (C) EdU incorporation assays of MCN1 *vs.* MCN1-C6. Error bars signify the mean ± SEM of three experimental replicates, with >1000 cells counted per sample for each replicate. (D) Representative images of tumors arising from transplantation of MCN1 (MT-R) and MCN1-C6 (MT-L) cells into cleared fad pads of recipient syngeneic FVB/N recipient females. MT-R and MT-L refer to right and left sides of mouse, respectively (see *Materials and Methods*). The right panel plots individual weights of tumors (n = 10 mice, 20 tumors).

Gilbert *et al.* 2014; Chavez *et al.* 2015; Konermann *et al.* 2015; Zhang *et al.* 2015).

Materials and Methods

Cancer cell lines

The 23116 MT cell line was generated from a primary MT that arose in a C3H-*Chaos3* mouse. The tumor was dissected and mechanical pulverized, then seeded on gelatin-coated culture dishes in Dulbecco's modified eagle medium (DMEM) supplemented with 10% fetal bovine serum (FBS). "Add-back" (AB) cell lines were generated by lentiviral transduction of *Arid1a* expression vector pLenti-puro-ARID1A (Addgene plasmid no. 39478), followed by puromycin selection (2 μg/ml) and growth of clonal lines (AB-C1/C2/C3) expressing ectopic *Arid1a*. All qRT-PCR primers are shown in Table S4.

aCGH

Genomic DNA was isolated from primary tumors by solubilizing in lysis buffer (50 mM Tris-HCl pH 8.0; 100 mM EDTA pH 8.0; 100 mM NaCl; 1% SDS; 0.5 mg/ml Proteinase K) for 3 hr at 55°, phenol/chloroform extraction, precipitation of the DNA in 0.8 volumes isopropanol, followed by spooling and washes in 70%, then 100% ethanol. One microgram of genomic DNA was used for labeling and hybridization to the SurePrint G3 Mouse Genome Comparative Genomic Hybridization (CGH) Microarray, 1 × 1 M (Agilent; product no. G4838A). Two independent reference WT DNAs (from strain C3HeB/FeJ mammary tissue) were used as hybridization controls. This array consists of 60-mer probes with an overall median spacing of 1.8 kb [1.5 kb in Reference Sequence (RefSeq) genes]. Content for probe design was sourced from University of California Santa Cruz (UCSC) mm9 (National Center for Biotechnology Information Build 37). DNA labeling, hybridization, and posthybridization processing were performed according to the manufacturer's protocol. Images were scanned using the Agilent's SureScan Microarray Scanner. Agilent's Cytogenomics software was used for spot identification and signal quantification, following normalization of test/reference ratios and background correction. Criteria for calling amplifications/deletions were as follows: minimum number of contiguous probes ≥3, minimum average absolute $\log_2$ ratio ≥0.25. Copy number alterations were visualized using the Integrative Genomics Viewer (IGV) software package (Robinson *et al.* 2011).

ddPCR

ddPCR was carried out using the QX200 Droplet Digital PCR System (Bio-Rad, Hercules, CA). Approximately 60 ng genomic DNA extracted from 51 different tumor samples (*Chaos3*-MTs and *Chaos3* non-MT controls) was used per reaction. Individual tumor samples were analyzed for copy number variations (CNVs) occurring in the target gene *Arid1a*, by probing two different genomic locations spanning the length of the entire gene. Primer and probe combinations used for the assay are shown in Table S4. *Gapdh* was used as a reference gene in CNV analyses. Droplet generation and droplet reading for ddPCR were carried out using Bio-Rad equipment and reagents, according to the manufacturer's instructions. Results were analyzed using QuantaSoft Software (Bio-Rad) and represented as concentration of DNA (copies per microliter). Each DNA sample was run in duplicate. Results for all samples analyzed are shown in Table S1.

qRT-PCR

Total RNA was isolated from cells and tissues using the E.Z.N.A. Total RNA Kit I (Omega Biotek). A total of 500 ng of RNA was used for cDNA synthesis using the qScript cDNA Supermix Kit (Quantabio). qRT-PCR analyses was done using Fast SYBR Green Master Mix (Life Technologies) and custom designed primers (Table S4), using GAPDH as an endogenous reference. Assays were run on the CFX96 Touch Real-Time PCR Detection System (Bio-Rad). Each sample was run in triplicate wells, from which mean Ct values were obtained. Relative quantification of gene expression was calculated using the ΔΔCt method. At least two technical replicates were run for each experiment to obtain standard error values.

EdU proliferation assay

Cells were grown overnight on coverslips and pulse labeled with 10 μM EdU for 30 min. Cells were then fixed with formaldehyde (final concentration of 1%) for 10 min, followed by permeabilization (0.3% Triton X-100 in PBS) for 15 min. The "Click" reaction cocktail [10 mM (+)-sodium-L-ascorbate; 0.1 mM 6-caboxyfluorescein-TEG azide; 2 mM CuSO4] was added to cells and incubated for 30 min at room temperature. Nuclei were counterstained with DAPI and coverslips were mounted on slides for EdU^+ cell counting by fluorescence microscopy. Experiments were conducted in triplicate, with >1000 cells counted per replicate.

Mammary fat pad injection surgeries

MT cell lines were injected into nos. 4 and 9 inguinal fat pads of 3-week-old nulliparous WT C3HeB/FeJ female mice, following clearance of the endogenous epithelium. Volume of cells injected per fat pad was 10 μl, at a concentration of 1×10^6 cells/ml. Tumors were allowed to develop until one grew to ~2 cm in diameter, at which point the animals were killed and tissues were collected for analyses. The time to tumor formation following surgery varied from 3 to 12 weeks.

Cell-cycle analyses

One million cells were centrifuged and resuspended in 200 μl of a cold hypotonic solution of propidium iodide (PI) (50 μg/ml PI, 1 mg/ml sodium citrate, and 1 μl/ml Triton X-100). Cells were incubated at 4° overnight for complete lysis and staining of nuclei. Cell-cycle profiles were analyzed using a flow cytometer (BD LSR II), with 488-nm excitation and emission collected with a 576/26 band-pass filter. Using a PI signal-specific width *vs.* area plot, only single nuclei were included in the analyses of all profiles.

Senescence-associated β-galactosidase assay

AB-C1 and 23116 MT cells were seeded onto a six-well dish at a concentration of 0.2×10^6 cells/ml. The next day, cells were stained using a senescence detection kit (Abcam, ab65351) as per the manufacturer's instructions. In brief, cells were fixed for 10 min at room temperature with the provided fixation solution and then stained for 16 hr at 37°. The next day, they were visualized using light microscopy for development of blue color. Images were taken at ×10 magnification and the number of positive cells were counted using ImageJ software. Experiments were carried out in triplicate to calculate the average percentage values.

RNA-seq

Total RNA was isolated from replicate samples of 23116 MT and AB clones (C1 and C2) cells using the E.Z.N.A. Total RNA Kit I. A total of 500 ng per sample was used to prepare cDNA libraries, with the NEBNext Poly(A) mRNA Magnetic Isolation Module and the NEBNext Ultra Directional RNA Library Prep Kit for Illumina (both from New England Biolabs). The libraries were then sequenced on Illumina's Hi-Seq platform, generating single-end 100-bp reads. Reads were aligned to the mouse genome (UCSC mm10) using Tophat v2.0.13 (Trapnell *et al.* 2012). Significant DE genes between 23116 MT and AB clones were determined with the help of the TopHat tool CuffDiff (v2.2.1), which uses a *Q*-value cutoff of 0.05 (*Q*-value = *P*-value corrected for multiple hypothesis testing) (Trapnell *et al.* 2012). DE genes were additionally sorted based on more stringent criteria where at least one condition (average of replicates) must have FPKM ≥5 and the minimum $\log_2$ (fold change) between conditions is twofold (up or down).

Data and reagent availability

Cell lines and constructs are available upon request. RNA-seq data and aCGH data are available at the Gene Expression Omnibus (accession nos. GSE81575 and GSE81967, respectively).

Acknowledgments

The authors are grateful to Alex Nikitin for providing MCN1 cells, Jennifer Grenier for the RNA-seq analysis, Christa Heyward and Rodica Bunaciu for assistance with flow cytometry, and Robert Weiss and Adrian McNairn for feedback on the manuscript. This work was supported by National Institutes of Health grant R21-CA175961 to J.C.S.

Literature Cited

American Cancer Society, 2014 Breast Cancer Facts and Figures 2015–2016. Available at cancer.org. Accessed June 21, 2016.

Andreasen, P. A., L. Kjoller, L. Christensen, and M. J. Duffy, 1997 The urokinase-type plasminogen activator system in cancer metastasis: a review. Int. J. Cancer 72: 1–22.

Bai, G., M. B. Smolka, and J. C. Schimenti, 2016 Chronic DNA replication stress reduces replicative lifespan of cells by TRP53-dependent, microRNA-assisted MCM2–7 downregulation. PLoS Genet. 12: e1005787.

Bitler, B. G., N. Fatkhutdinov, and R. Zhang, 2015 Potential therapeutic targets in ARID1A-mutated cancers. Expert Opin. Ther. Targets 19: 1419–1422.

Bosse, T., N. T. ter Haar, L. M. Seeber, P. J. v Diest, F. J. Hes *et al.*, 2013 Loss of ARID1A expression and its relationship with PI3K-Akt pathway alterations, TP53 and microsatellite instability in endometrial cancer. Mod. Pathol. 26: 1525–1535.

Bunz, F., A. Dutriaux, C. Lengauer, T. Waldman, S. Zhou *et al.*, 1998 Requirement for p53 and p21 to sustain G2 arrest after DNA damage. Science 282: 1497–1501.

Butt, A. J., K. A. Dickson, F. McDougall, and R. C. Baxter, 2003 Insulin-like growth factor-binding protein-5 inhibits the growth of human breast cancer cells in vitro and in vivo. J. Biol. Chem. 278: 29676–29685.

Cajuso, T., U. A. Hanninen, J. Kondelin, A. E. Gylfe, T. Tanskanen *et al.*, 2014 Exome sequencing reveals frequent inactivating mutations in ARID1A, ARID1B, ARID2 and ARID4A in microsatellite unstable colorectal cancer. Int. J. Cancer 135: 611–623.

Chandler, R. L., J. Brennan, J. C. Schisler, D. Serber, C. Patterson *et al.*, 2013 ARID1a-DNA interactions are required for promoter occupancy by SWI/SNF. Mol. Cell. Biol. 33: 265–280.

Chandler, R. L., J. S. Damrauer, J. R. Raab, J. C. Schisler, M. D. Wilkerson *et al.*, 2015 Coexistent ARID1A–PIK3CA mutations promote ovarian clear-cell tumorigenesis through pro-tumorigenic inflammatory cytokine signalling. Nat. Commun. 6: 6118.

Chavez, A., J. Scheiman, S. Vora, B. W. Pruitt, M. Tuttle *et al.*, 2015 Highly efficient Cas9-mediated transcriptional programming. Nat. Methods 12: 326–328.

Cheng, L., Z. Zhou, A. Flesken-Nikitin, I. A. Toshkov, W. Wang *et al.*, 2010 Rb inactivation accelerates neoplastic growth and substitutes for recurrent amplification of cIAP1, cIAP2 and Yap1 in sporadic mammary carcinoma associated with p53 deficiency. Oncogene 29: 5700–5711.

Cho, H. D., J. E. Lee, H. Y. Jung, M. H. Oh, J. H. Lee *et al.*, 2015 Loss of tumor suppressor ARID1A protein expression correlates with poor prognosis in patients with primary breast cancer. J. Breast Cancer 18: 339–346.

Chuang, C. H., D. Yang, G. Bai, A. Freeland, S. C. Pruitt *et al.*, 2012 Post-transcriptional homeostasis and regulation of MCM2–7 in mammalian cells. Nucleic Acids Res. 40: 4914–4924.

Ciriello, G., M. L. Gatza, A. H. Beck, M. D. Wilkerson, S. K. Rhie *et al.*, 2015 Comprehensive molecular portraits of invasive lobular breast cancer. Cell 163: 506–519.

Cornen, S., J. Adelaide, F. Bertucci, P. Finetti, A. Guille *et al.*, 2012 Mutations and deletions of ARID1A in breast tumors. Oncogene 31: 4255–4256.

Eirew, P., A. Steif, J. Khattra, G. Ha, D. Yap *et al.*, 2015 Dynamics of genomic clones in breast cancer patient xenografts at single-cell resolution. Nature 518: 422–426.

Gao, X., P. Tate, P. Hu, R. Tjian, W. C. Skarnes *et al.*, 2008 ES cell pluripotency and germ-layer formation require the SWI/SNF chromatin remodeling component BAF250a. Proc. Natl. Acad. Sci. USA 105: 6656–6661.

Gilbert, L. A., M. A. Horlbeck, B. Adamson, J. E. Villalta, Y. Chen *et al.*, 2014 Genome-scale CRISPR-mediated control of gene repression and activation. Cell 159: 647–661.

Guan, B., T. L. Wang, and M. Shih Ie, 2011 ARID1A, a factor that promotes formation of SWI/SNF-mediated chromatin remodeling, is a tumor suppressor in gynecologic cancers. Cancer Res. 71: 6718–6727.

Guan, B., Y. S. Rahmanto, R. C. Wu, Y. Wang, Z. Wang *et al.*, 2014 Roles of deletion of Arid1a, a tumor suppressor, in mouse ovarian tumorigenesis. J. Natl. Cancer Inst. Avalable at: http://jnci.oxfordjournals.org/content/106/7/dju146.full.

Imielinski, M., A. H. Berger, P. S. Hammerman, B. Hernandez, T. J. Pugh *et al.*, 2012 Mapping the hallmarks of lung adenocarcinoma with massively parallel sequencing. Cell 150: 1107–1120.

Inoue, H., S. Giannakopoulos, C. N. Parkhurst, T. Matsumura, E. A. Kono *et al.*, 2011 Target genes of the largest human SWI/SNF complex subunit control cell growth. Biochem. J. 434: 83–92.

Jones, S., T. L. Wang, M. Shih Ie, T. L. Mao, K. Nakayama *et al.*, 2010 Frequent mutations of chromatin remodeling gene ARID1A in ovarian clear cell carcinoma. Science 330: 228–231.

Kandoth, C., M. D. McLellan, F. Vandin, K. Ye, B. Niu *et al.*, 2013 Mutational landscape and significance across 12 major cancer types. Nature 502: 333–339.

Kawabata, T., S. W. Luebben, S. Yamaguchi, I. Ilves, I. Matise *et al.*, 2011 Stalled fork rescue via dormant replication origins in unchallenged S phase promotes proper chromosome segregation and tumor suppression. Mol. Cell 41: 543–553.

Kim, K. S., Y. B. Seu, S. H. Baek, M. J. Kim, K. J. Kim *et al.*, 2007 Induction of cellular senescence by insulin-like growth factor binding protein-5 through a p53-dependent mechanism. Mol. Biol. Cell 18: 4543–4552.

Konermann, S., M. D. Brigham, A. E. Trevino, J. Joung, O. O. Abudayyeh *et al.*, 2015 Genome-scale transcriptional activation by an engineered CRISPR-Cas9 complex. Nature 517: 583–588.

Krenning, L., F. M. Feringa, I. A. Shaltiel, J. van den Berg, and R. H. Medema, 2014 Transient activation of p53 in G2 phase is sufficient to induce senescence. Mol. Cell 55: 59–72.

Kuilman, T., C. Michaloglou, W. J. Mooi, and D. S. Peeper, 2010 The essence of senescence. Genes Dev. 24: 2463–2479.

Liang, H., L. W. Cheung, J. Li, Z. Ju, S. Yu *et al.*, 2012 Whole-exome sequencing combined with functional genomics reveals novel candidate driver cancer genes in endometrial cancer. Genome Res. 22: 2120–2129.

Lobrich, M., and P. A. Jeggo, 2007 The impact of a negligent G2/M checkpoint on genomic instability and cancer induction. Nat. Rev. Cancer 7: 861–869.

Maeda, D., and M. Shih Ie, 2013 Pathogenesis and the role of ARID1A mutation in endometriosis-related ovarian neoplasms. Adv. Anat. Pathol. 20: 45–52.

Maeder, M. L., J. F. Angstman, M. E. Richardson, S. J. Linder, V. M. Cascio *et al.*, 2013 Targeted DNA demethylation and activation of endogenous genes using programmable TALE-TET1 fusion proteins. Nat. Biotechnol. 31: 1137–1142.

Mamo, A., L. Cavallone, S. Tuzmen, C. Chabot, C. Ferrario *et al.*, 2012 An integrated genomic approach identifies ARID1A as a candidate tumor-suppressor gene in breast cancer. Oncogene 31: 2090–2100.

Mao, Z., Z. Ke, V. Gorbunova, and A. Seluanov, 2012 Replicatively senescent cells are arrested in G1 and G2 phases. Aging (Albany, NY) 4: 431–435.

Pereira, J. J., T. Meyer, S. E. Docherty, H. H. Reid, J. Marshall *et al.*, 2004 Bimolecular interaction of insulin-like growth factor (IGF) binding protein-2 with alphavbeta3 negatively modulates IGF-I-mediated migration and tumor growth. Cancer Res. 64: 977–984.

Robinson, J. T., H. Thorvaldsdottir, W. Winckler, M. Guttman, E. S. Lander *et al.*, 2011 Integrative genomics viewer. Nat. Biotechnol. 29: 24–26.

Romero, O. A., and M. Sanchez-Cespedes, 2014 The SWI/SNF genetic blockade: effects in cell differentiation, cancer and developmental diseases. Oncogene 33: 2681–2689.

Shen, J., Y. Peng, L. Wei, W. Zhang, L. Yang *et al.*, 2015 ARID1A deficiency impairs the DNA damage checkpoint and sensitizes cells to PARP inhibitors. Cancer Discov. 5: 752–767.

Shima, N., A. Alcaraz, I. Liachko, T. R. Buske, C. A. Andrews *et al.*, 2007 A viable allele of Mcm4 causes chromosome instability and mammary adenocarcinomas in mice. Nat. Genet. 39: 93–98.

The Cancer Genome Atlas Network, 2012 Comprehensive molecular portraits of human breast tumours. Nature 490: 61–70.

The Cancer Genome Atlas Research Network; C. Kandoth, N. Schultz, A. D. Cherniack, R. Akbani *et al.*, 2013 Integrated genomic characterization of endometrial carcinoma. Nature 497: 67–73.

Trapnell, C., A. Roberts, L. Goff, G. Pertea, D. Kim *et al.*, 2012 Differential gene and transcript expression analysis of RNA-seq experiments with TopHat and Cufflinks. Nat. Protoc. 7: 562–578.

Waddell, N., M. Pajic, A. M. Patch, D. K. Chang, K. S. Kassahn *et al.*, 2015 Whole genomes redefine the mutational landscape of pancreatic cancer. Nature 518: 495–501.

Wallace, M. D., A. D. Pfefferle, L. Shen, A. J. McNairn, E. G. Cerami *et al.*, 2012 Comparative oncogenomics implicates the neurofibromin 1 gene (NF1) as a breast cancer driver. Genetics 192: 385–396.

Wallace, M. D., T. L. Southard, K. J. Schimenti, and J. C. Schimenti, 2014 Role of DNA damage response pathways in preventing carcinogenesis caused by intrinsic replication stress. Oncogene 33: 3688–3695.

Wang, K., J. Kan, S. T. Yuen, S. T. Shi, K. M. Chu *et al.*, 2011 Exome sequencing identifies frequent mutation of ARID1A in molecular subtypes of gastric cancer. Nat. Genet. 43: 1219–1223.

Wiegand, K. C., S. P. Shah, O. M. Al-Agha, Y. Zhao, K. Tse *et al.*, 2010 ARID1A mutations in endometriosis-associated ovarian carcinomas. N. Engl. J. Med. 363: 1532–1543.

Wu, R. C., T. L. Wang, and M. Shih Ie, 2014 The emerging roles of ARID1A in tumor suppression. Cancer Biol. Ther. 15: 655–664.

Zang, Z. J., I. Cutcutache, S. L. Poon, S. L. Zhang, J. R. McPherson *et al.*, 2012 Exome sequencing of gastric adenocarcinoma identifies recurrent somatic mutations in cell adhesion and chromatin remodeling genes. Nat. Genet. 44: 570–574.

Zhang, Y., C. Yin, T. Zhang, F. Li, W. Yang *et al.*, 2015 CRISPR/gRNA-directed synergistic activation mediator (SAM) induces specific, persistent and robust reactivation of the HIV-1 latent reservoirs. Sci. Rep. 5: 16277.

Zhao, J., C. Liu, and Z. Zhao, 2014 ARID1A: a potential prognostic factor for breast cancer. Tumour Biol. 35: 4813–4819.

Communicating editor: T. R. Magnuson

GENETICS

Supporting Information
www.genetics.org/lookup/suppl/doi:10.1534/genetics.115.184879/-/DC1

The Chromatin Remodeling Component *Arid1a* Is a Suppressor of Spontaneous Mammary Tumors in Mice

Nithya Kartha, Lishuang Shen, Carolyn Maskin, Marsha Wallace, and John C. Schimenti

DOI: 10.1534/genetics.115.184879

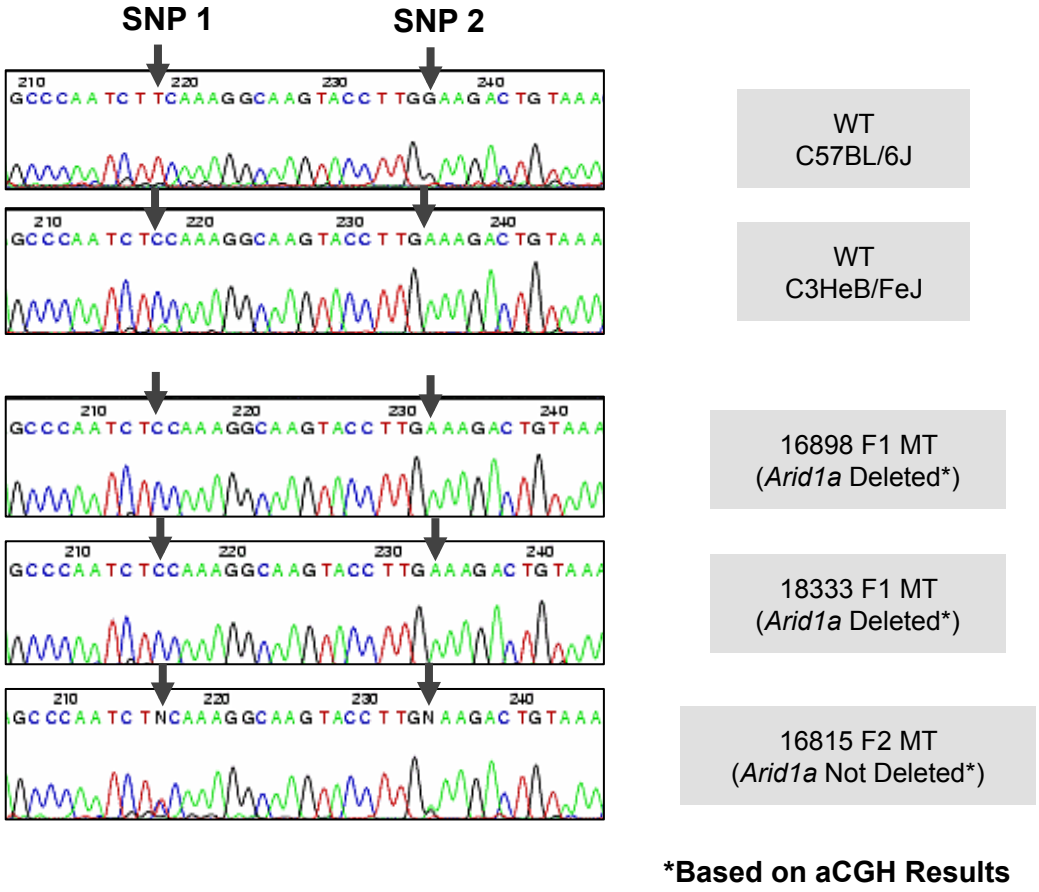

Figure S1. **SNP Genotyping of *Chaos3*-MTs.** Three individual *Arid1a* SNPs specific to C3HeB/FeJ and C57BL/6J strains were genotyped in F1 and F2 MTs derived from mice generated by crossing these two strains, for which aCGH analyses was also conducted.

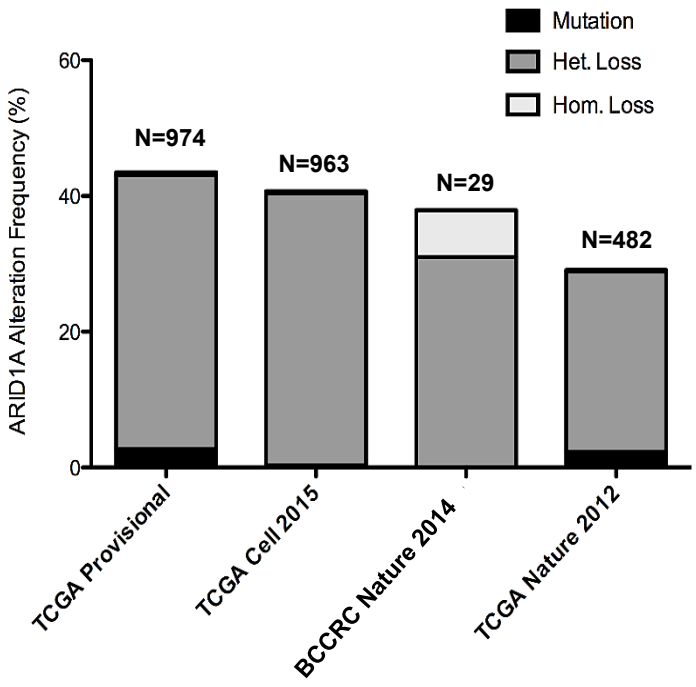

Fig. S2. *ARID1A* copy number in human breast cancers. Data and analytical tools from the cBio portal (http://www.cbioportal.org) were used for generating the graph. “Mutation” refers to intragenic mutations such as point changes; “Het. Loss” = 1 *ARID1A* copy scored as missing; “Hom. Loss” = no *ARID1A* copies remaining.

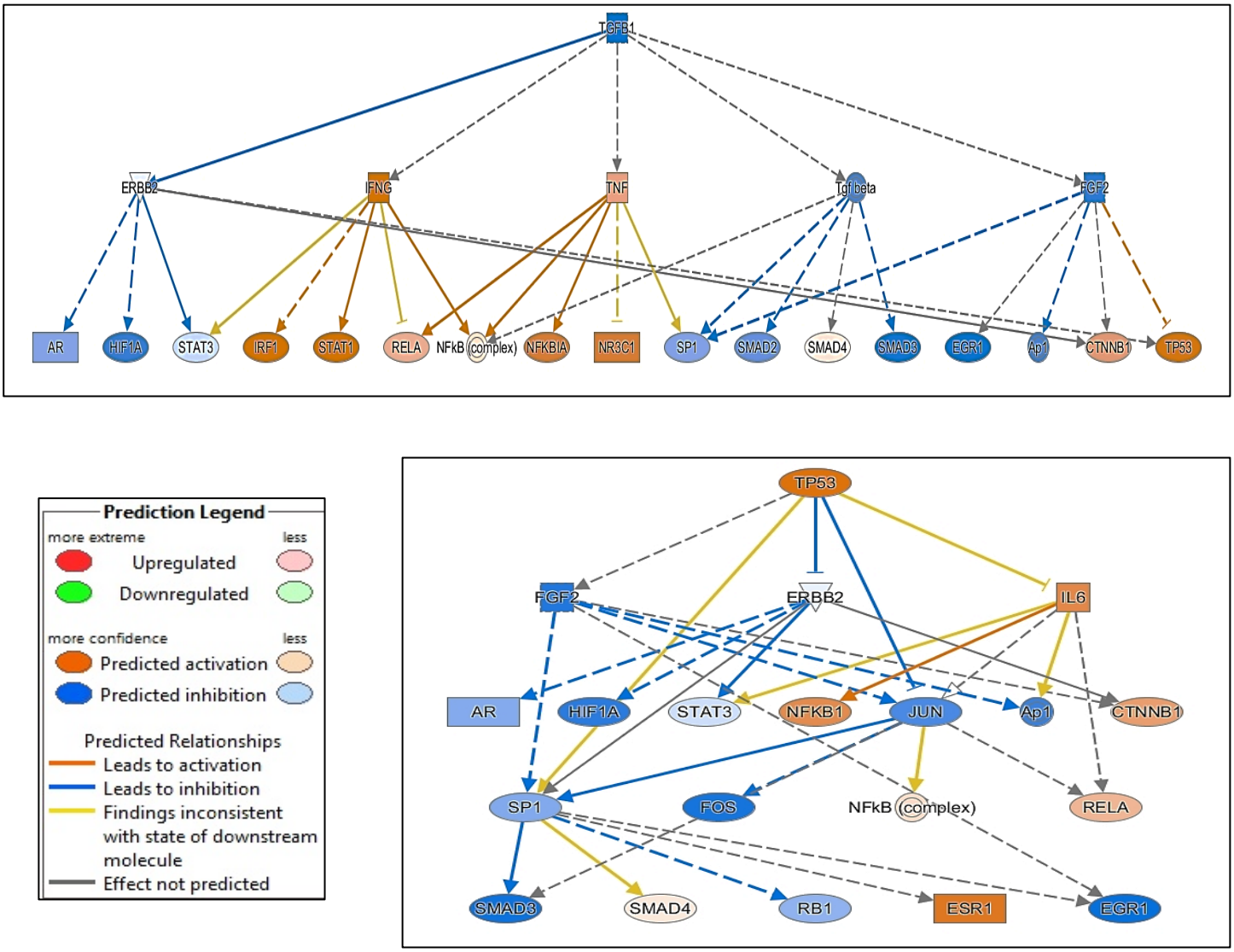

Figure S3: IPA Analyses of RNA-Seq DE Genes. Ingenuity Pathway Analyses of gene networks altered within the TGFB1 and TP53 pathways in AB-C1and AB-C2 cells.

Table S1. *Arid1a* CNVs across C3H-Chaos3 MTs and controls determined by ddPCR.

(.xlsx, 25 KB)

Available for download as a .xlsx file at
www.genetics.org/lookup/suppl/doi:10.1534/genetics.115.184879/-/DC1/TableS1.xlsx

Table S2. Comparison of *Arid1a* CNVs and Expression across Individual *Chaos3* MTs.

(.xlsx, 12 KB)

Available for download as a .xlsx file at
www.genetics.org/lookup/suppl/doi:10.1534/genetics.115.184879/-/DC1/TableS2.xlsx

Table S3. Differentially Expressed Genes (23116 MT vs AB-C1). (.xlsx, 31 KB)

Available for download as a .xlsx file at
www.genetics.org/lookup/suppl/doi:10.1534/genetics.115.184879/-/DC1/TableS3.xlsx

Table S4. Primer Sequences. (.xlsx, 11 KB)

Available for download as a .xlsx file at
www.genetics.org/lookup/suppl/doi:10.1534/genetics.115.184879/-/DC1/TableS4.xlsx